

GRAVITATIONAL COLLAPSE OF MAGNETIZED CLOUDS

I. IDEAL MHD ACCRETION FLOW

Daniele Galli

*INAF-Osservatorio Astrofisico di Arcetri
Largo Enrico Fermi 5, I-50125 Firenze, Italy
galli@arcetri.astro.it*

Susana Lizano

*Centro de Radioastronomía y Astrofísica, UNAM
Apdo. Postal 3-72, Morelia, Michoacán 58089, Mexico
s.lizano@astrosmo.unam.mx*

Frank H. Shu

*Physics Department, National Tsing Hua University
Hsinchu 30013, Taiwan, Republic of China
shu@mx.nthu.edu.tw*

Anthony Allen

*Institute of Astronomy and Astrophysics
Academia Sinica, Taipei 106, Republic of China
tony@asiaa.sinica.edu.tw*

ABSTRACT

We study the self-similar collapse of an isothermal magnetized rotating cloud in the ideal magnetohydrodynamic (MHD) regime. In the limit of small distance from the accreting protostar we find an analytic solution that corresponds to free-fall onto a central mass point. The density distribution is not spherically symmetric but depends on the mass loading of magnetic field lines, which can be obtained by matching our inner solution to an outer collapse solution previously computed by Allen, Shu & Li. The concentration of magnetic field trapped by the central mass point under field-freezing, independent on the details of the starting state, creates a split monopole configuration where the magnetic field strength increases as the inverse square of the distance from the center. Under such conditions, the inflow eventually becomes subalfvènic and the outward transfer

of angular momentum by magnetic braking very efficient, thus preventing the formation of a centrifugally supported disk. Instead, the azimuthal velocity of the infalling gas decreases to zero at the center, and the gas spirals into the star. Therefore, the dissipation of dynamically important levels of magnetic field is a fundamental requisite for the formation of protoplanetary disks around young stars.

Subject headings: ISM:clouds — ISM: magnetic fields — magnetohydrodynamics — planetary systems: protoplanetary disks — stars: formation

1. Introduction

Since the realization that magnetic fields exist in interstellar clouds, there has been the potential for a severe magnetic-flux problem in star formation. If field freezing were to apply (the ideal MHD conditions), newly formed solar-type stars should have surface fields of $\sim 10^7$ G (e.g., Mestel & Spitzer 1956), which is several thousand times larger than given by the observations of T Tauri stars (e.g., Johns-Krull, Valenti, & Saar 2004). Magnetic-field dissipation is crucial to the resolution of this contradiction. In this paper, we demonstrate that it is also needed to avoid an extremely efficient magnetic braking that would prevent the formation of the observed protoplanetary disks around young stars.

Allen, Shu & Li (2003; hereafter A03a) performed informative numerical simulations of the collapse of isothermal magnetized toroids, which are axially symmetric equilibrium configurations with spatially uniform mass-to-flux ratio (such configuration is called *isopedic*). These are pivotal states at time $t = 0$, in the sense that they represent the idealized state of a molecular cloud core at the instant of formation of a central density cusp, and separate the pre-protostellar phase of evolution from the protostellar accretion phase (Li & Shu 1996). The structure of these toroids is completely determined by the single parameter H_0 , that is the fraction of support provided against self-gravity by poloidal magnetic fields relative to that of gas pressure (Li & Shu 1996). The collapse of singular isothermal toroids occurs inside-out in a self-similar manner (A03a), in which matter collapses toward the central point mass dragging magnetic field lines along with it.

Later, Allen, Li & Shu (2003; hereafter A03b) included angular momentum characterized by a flat rotation curve in these models. The formation of a centrifugally supported disk around the central star did not occur for any reasonable nonzero value of the magnetic support parameter H_0 . They concluded that, in ideal MHD conditions (i.e., no magnetic field dissipation), the efficiency of magnetic braking was so high as to prevent disk forma-

tion. Simulations with limited numerical resolution can be suggestive, but proof requires an analytic or semi-analytic demonstration. Analytic or semi-analytic results have the added advantage that they can be the starting points for additional development, such as providing a background equatorial collapse against which a bipolar outflow might simultaneously be taking place along the poles (Lizano et al. 2006, in preparation), or for an extension into the non-ideal regime (Shu et al. 2006).

Motivated by these considerations, in this paper we determine analytically the asymptotic behavior of the density, velocity and magnetic field in the self-similar collapse of an isothermal magnetized rotating cloud. We find that at small scales the density and poloidal velocity field in the collapse solution approaches free-fall on a split magnetic monopole configuration, with the azimuthal velocity decreasing to zero at the origin. This result proves that, without magnetic field dissipation, a centrifugally supported disk around the accreting central star cannot form.

The organization of the paper is as follows. In §2 we discuss the relevant ideal MHD equations. In §3 we put these equations in non-dimensional self-similar form. In §4 we write the self-similar equations in a streamline formulation, in terms of the Grad-Shafranov and Bernoulli’s equation, and take the limit for small values of the self-similar variable $x = r/at$, where r is the spherical radius, a is the sound speed of the cloud and t is the time variable. In §5 we show some numerical examples of our inner solution for the case of no rotation, using the numerical simulations of A03a to obtain an approximation for the mass loading of field lines. In §6 we consider the effects of rotation and show that the azimuthal velocity vanishes at the origin, i.e., the efficient magnetic braking prevents the formation of a centrifugally disk around the star. Finally, in §8, we discuss the implications of our work and summarize our conclusions.

2. Ideal MHD equations

The equations governing the collapse of an isothermal magnetized cloud are the equation of continuity

$$\frac{\partial \rho}{\partial t} + \nabla \cdot (\rho \mathbf{u}) = 0, \quad (1)$$

where ρ is the density and \mathbf{u} is the velocity of the gas; the equation of motion

$$\frac{\partial \mathbf{u}}{\partial t} + (\nabla \times \mathbf{u}) \times \mathbf{u} + \frac{1}{2} \nabla |\mathbf{u}|^2 = -\frac{a^2}{\rho} \nabla \rho - \nabla V + \frac{1}{4\pi\rho} (\nabla \times \mathbf{B}) \times \mathbf{B}, \quad (2)$$

where V is the gravitational potential and \mathbf{B} is the magnetic field, the induction equation in the ideal MHD limit

$$\frac{\partial \mathbf{B}}{\partial t} = \nabla \times (\mathbf{u} \times \mathbf{B}), \quad (3)$$

the condition of no monopoles,

$$\nabla \cdot \mathbf{B} = 0, \quad (4)$$

and Poisson's equation

$$\nabla^2 V = 4\pi G \rho, \quad (5)$$

where G is the gravitational constant.

The geometry of the collapse is shown in Figure 1. A separatrix indicated in dashed lines separates field lines which have been pulled into the origin by the inflow from field lines tied to matter in the infalling envelope (see, e.g., Figures 4, 6 and 7 of A03a). We will study only the region inside the separatrix surface that is close to the origin (within the dotted circle in Figure 1).

3. Self-similar variables

Since the singular isothermal toroids defining the pivotal $t = 0$ states are self-similar, we look for collapse solutions depending only on the similarity coordinate \mathbf{x} , defined by

$$\mathbf{r} = at\mathbf{x}. \quad (6)$$

We introduce appropriate nondimensional (reduced) variables defined as

$$\rho(\mathbf{r}, t) = \frac{1}{4\pi G t^2} \alpha(\mathbf{x}), \quad (7)$$

$$\mathbf{u}(\mathbf{r}, t) = a\mathbf{v}(\mathbf{x}), \quad (8)$$

$$V(\mathbf{r}, t) = a^2 \Psi(\mathbf{x}), \quad (9)$$

$$\mathbf{B}(\mathbf{r}, t) = \frac{a}{G^{1/2} t} \mathbf{b}(\mathbf{x}). \quad (10)$$

Inserting the definitions (6)–(10) into eq. (1)–(3), we obtain the set of nondimensional equations governing the self-similar collapse,

$$(\mathbf{v} - \mathbf{x}) \cdot \nabla \alpha + \alpha \nabla \cdot \mathbf{v} = 2\alpha, \quad (11)$$

$$-(\mathbf{x} \cdot \nabla) \mathbf{v} + (\nabla \times \mathbf{v}) \times \mathbf{v} + \frac{1}{2} \nabla |\mathbf{v}|^2 = -\frac{1}{\alpha} \nabla \alpha - \nabla \Psi + \frac{1}{\alpha} (\nabla \times \mathbf{b}) \times \mathbf{b}, \quad (12)$$

$$-(\mathbf{x} \cdot \nabla) \mathbf{b} = \mathbf{b} + \nabla \times (\mathbf{v} \times \mathbf{b}), \quad (13)$$

$$\nabla \cdot \mathbf{b} = 0, \quad (14)$$

$$\nabla^2 \Psi = \alpha. \quad (15)$$

4. The inner limit

In the limit $|\mathbf{x}| \ll 1$ we approximate for any vector or scalar variable \mathbf{f} ,

$$\mathbf{f} \sim (\mathbf{x} \cdot \nabla) \mathbf{f} \ll (\mathbf{v} \cdot \nabla) \mathbf{f}. \quad (16)$$

With these approximations, eq. (11)–(13) become

$$\nabla \cdot (\alpha \mathbf{v}) = 0, \quad (17)$$

$$(\nabla \times \mathbf{v}) \times \mathbf{v} + \frac{1}{2} \nabla |\mathbf{v}|^2 = -\frac{1}{\alpha} \nabla \alpha - \nabla \Psi + \frac{1}{\alpha} (\nabla \times \mathbf{b}) \times \mathbf{b}, \quad (18)$$

$$\nabla \times (\mathbf{v} \times \mathbf{b}) = 0. \quad (19)$$

These equations for the self-similar variables in the inner region are formally equivalent to the dimensional equations of steady, ideal MHD flow. The time-dependent self-similar flow becomes quasi-steady when the time it takes the flow to cross the inner region becomes small compared to the evolutionary time governing changes of the infall envelope that feeds matter and field into the inner regions. The latter condition holds independent of the starting assumption of self-similarity of the overall collapse (see e.g. Galli & Shu 1993b), and therefore our results have greater generality than its formal derivation here. In the steady-flow approximation, we may profitably introduce a streamline formalism (e.g, Shafranov 1966; Shu al. 1994).

In the following we adopt spherical coordinates (x, θ, φ) , and assume that the system is axisymmetric ($\partial/\partial\varphi = 0$). Then eq. (17) is satisfied introducing a stream function $\psi(\mathbf{x})$ such that

$$\alpha \mathbf{v}_p = \nabla \times \left[\frac{\psi}{x \sin \theta} \hat{\mathbf{e}}_\varphi \right], \quad (20)$$

where the components of the poloidal velocity \mathbf{v}_p are

$$v_x = \frac{1}{\alpha x^2 \sin \theta} \frac{\partial \psi}{\partial \theta} \quad \text{and} \quad v_\theta = -\frac{1}{\alpha x \sin \theta} \frac{\partial \psi}{\partial x}. \quad (21)$$

Reflection symmetry requires ψ to be an odd function of θ with respect to $\theta = \pi/2$, therefore

$$\psi \left(x, \frac{\pi}{2} \right) = 0. \quad (22)$$

Imposing that the integral over solid angle of the mass flow $-r^2 \rho u_r$ gives the accretion rate $\dot{M} = m_0(1 + H_0)a^3/G$, where $m_0 = 0.975$ is the reduced mass at the origin (Li & Shu 1997), we obtain the condition

$$\psi(x, 0) = m_0(1 + H_0). \quad (23)$$

Thus, the value of $\psi/\psi(x, 0)$ is the fraction of the accretion rate carried by the streamlines from $-\psi$ to ψ .

Eq. (19) implies that $\mathbf{v} \parallel \mathbf{b}$. We define the function β , related to the mass loading of field lines, by

$$\mathbf{b} = \beta \alpha \mathbf{v}. \quad (24)$$

Using this definition, the condition of no monopoles, eq. (14), and the equation of continuity, eq. (17), one obtains

$$\mathbf{v} \cdot \nabla \beta = 0, \quad (25)$$

i.e., $\beta = \beta(\psi)$, is constant along streamlines. We note that β is antisymmetric with respect to the equatorial plane (by convention, β negative corresponds to the upper hemisphere).

If we dot the force equation (18) with \mathbf{v} we obtain Bernoulli's equation

$$\frac{1}{2}|\mathbf{v}|^2 + \ln \alpha + \Psi = H(\psi), \quad (26)$$

where $H(\psi)$ is Bernoulli's function which is constant on streamlines. Substituting this equation and using the definition of β , eq. (24), in the equation of motion, eq. (18), we obtain after collecting terms,

$$H' \nabla \psi + [\nabla \times (1 - \alpha \beta^2) \mathbf{v} + \nabla \beta \times \beta \alpha \mathbf{v}] \times \mathbf{v} = 0, \quad (27)$$

where a prime denotes differentiation with respect to ψ . We now decompose this equation along $\hat{\mathbf{e}}_\varphi$ and $\nabla \psi$.

After some algebra, one can write the poloidal component of eq. (27) as

$$\left(H' + \frac{\omega}{\alpha x \sin \theta} - \frac{v_\varphi}{x \sin \theta} j' - \alpha \beta \beta' |\mathbf{v}|^2 \right) \nabla \psi = 0, \quad (28)$$

where

$$\omega \hat{\mathbf{e}}_\varphi \equiv \nabla \times (1 - \alpha \beta^2) \mathbf{v}_p \quad (29)$$

is the total vorticity. For nontrivial solutions of this equation to exist, we require

$$H' + \frac{\omega}{\alpha x \sin \theta} - \frac{v_\varphi}{x \sin \theta} j' - \beta \beta' \alpha |\mathbf{v}|^2 = 0, \quad (30)$$

which is a form of the Grad-Shafranov (G-S) equation that expresses the condition of force balance across field lines. We can write the total vorticity as

$$\omega = -\frac{1}{x \sin \theta} \left[A \mathcal{S}(\psi) - 2\beta \beta' |\nabla \psi|^2 - \frac{1}{\alpha^2} \nabla \alpha \cdot \nabla \psi \right], \quad (31)$$

where \mathcal{S} is the Stokes operator

$$\mathcal{S}(\psi) = \frac{\partial^2 \psi}{\partial x^2} + \frac{1}{x^2} \frac{\partial^2 \psi}{\partial \theta^2} - \frac{\cot \theta}{x^2} \frac{\partial \psi}{\partial \theta}, \quad (32)$$

and A is the Alfvèn discriminant

$$A = \frac{1 - \alpha \beta^2}{\alpha}. \quad (33)$$

Then, the G-S equation, (30), can be written as

$$A \mathcal{S}(\psi) = \alpha H' x^2 \sin^2 \theta + \frac{1}{\alpha^2} \nabla \alpha \cdot \nabla \psi - \frac{1}{A} j j' + \beta \beta' |\nabla \psi|^2. \quad (34)$$

The toroidal component of equation (27) is

$$\mathbf{v} \cdot (\nabla j + \alpha \beta v_\varphi \nabla \beta) = 0, \quad (35)$$

where we have defined the total (gas plus magnetic field) specific angular momentum

$$j \equiv x \sin \theta (1 - \alpha \beta^2) v_\varphi. \quad (36)$$

Since β is constant along streamlines by eq. (25), eq. (35) reduces to

$$\mathbf{v} \cdot \nabla j = 0, \quad (37)$$

stating that $j = j(\psi)$ is constant along streamlines. Thus, the toroidal velocity is given by

$$v_\varphi = \frac{j(\psi)}{x \sin \theta (1 - \alpha \beta^2)}. \quad (38)$$

Notice the formal singular point that arises when $\alpha \beta^2 = 1$, which is the condition of the poloidal velocity reaching the Alfvèn speed. In fact, the smooth crossing of this surface (with a continuously varying v_φ) is made in a time-dependent way; as will be shown in Sect. 5, the poloidal velocity is distinctly subalfvènic ($\alpha \beta^2 \gg 1$) in the steady part of the flow. Finally, Bernoulli's eq. (26) can be rewritten as

$$|\nabla \psi|^2 + \left(\frac{j}{A} \right)^2 + 2\alpha^2 x^2 \sin^2 \theta (\ln \alpha + \Psi - H) = 0. \quad (39)$$

Thus, in the inner limit, the ideal MHD equations of the problem (17)–(19), can be reduced to the G-S and Bernoulli's equations (eq. 34 and 39, respectively). These need to be solved for the stream function ψ and the density α (or the Alfvèn discriminant A), given the functions $H(\psi)$, $j(\psi)$, and $\beta(\psi)$, which are quantities conserved along streamlines. Then, the toroidal components of the magnetic field and the velocity can be obtained from eq. (24) and (38), respectively.

5. Case of no rotation ($j = 0$)

We first consider the case of no rotation, and we look for a separable solution in spherical coordinates in which all variables have a power-law dependence on x . One can show that the density and the stream function must have forms that represent magnetically-modulated free-fall solutions:

$$\alpha(x, \theta) = \left[\frac{m_0(1 + H_0)}{2} \right]^{1/2} x^{-3/2} Q(\theta), \quad (40)$$

and

$$\psi(x, \theta) = m_0(1 + H_0)f(\theta), \quad (41)$$

where $Q(\theta)$ is normalized so that

$$\int_0^{\pi/2} Q(\theta) \sin \theta d\theta = 1. \quad (42)$$

The angular part of the stream function, $f(\theta)$, is normalized so that $f(0) = 1$ and $f(\pi/2) = 0$, i.e., the streamlines between those falling in equatorially and along the pole carry the entire mass infall rate of the upper hemisphere.

To find the unknown functions $Q(\theta)$ and $f(\theta)$ we need to balance the highest order terms in eqs. (34) and (39). The dominant terms that balance in the G-S equation, eq. (34), are then

$$-\beta^2 \mathcal{S}(\psi) \approx \beta \beta' |\nabla \psi|^2, \quad (43)$$

where the Alfvèn discriminant, $A \approx -\beta^2$, corresponds to highly subalfvènic poloidal flow.

In Bernoulli's equation the dominant terms that balance are the poloidal kinetic energy and the gravitational potential energy. With the gravitational potential of a point mass at the origin, $\Psi = -m_0(1 + H_0)/x$, we get

$$|\nabla \psi|^2 \approx 2m_0(1 + H_0)\alpha^2 x \sin^2 \theta. \quad (44)$$

Substituting the definitions (40) and (41) in this latter equation, one gets

$$\frac{df}{d\theta} = -Q(\theta) \sin \theta. \quad (45)$$

The G-S equation (43) now becomes a second-order, nonlinear, ordinary differential equation for $f(\theta)$,

$$\frac{d^2 f}{d\theta^2} - \cot \theta \frac{df}{d\theta} + \frac{\beta'}{\beta} \left(\frac{df}{d\theta} \right)^2 = 0. \quad (46)$$

Combining the Bernoulli equation (45) and the G-S equation (46), one obtains

$$\frac{dQ}{df} = -\frac{\beta'}{\beta}Q, \quad (47)$$

which has the solution

$$Q(f) = \frac{\bar{\beta}}{\beta(f)}, \quad (48)$$

where $\bar{\beta}$ is an integration constant. Furthermore, $f(\theta)$ has the parametric solution

$$\cos \theta(f) = \frac{1}{\bar{\beta}} \int_0^f \beta(f) df, \quad (49)$$

where we have used the B.C. $f(\pi/2) = 0$. Moreover, the B.C. $f(0) = 1$, implies that

$$\bar{\beta} = \int_0^1 \beta(f) df. \quad (50)$$

The physical meaning of the above results is simple. Equation (49) implies that the poloidal field lines spread so as to distribute themselves uniformly in polar angle, i.e., the magnetic configuration takes the shape of a *split monopole*, as anticipated by Galli & Shu (1993a; see their Figure 2) and confirmed later by Li & Shu (1997) for the collapse of an infinitesimally thin disk. This happens because the field lines trapped in the central mass point become so strong that the mass inflow, being highly subalfvénic, is unable to bend them from the zeroth-order vacuum field configuration. In turn, the matter is constrained by field freezing to flow along the radial field lines, and the density distribution is that appropriate for free-fall along each radial path (eq. 41), but it departs from a homogenous angular distribution in a manner that depends only on the initial mass-to-flux loading (eq. 48).

Given the above interpretation, it is useful to define the magnetic flux function

$$\Phi(\mathbf{r}, t) = \frac{2\pi a^3 t}{G^{1/2}} \phi(\mathbf{x}), \quad (51)$$

from which we may obtain the poloidal field \mathbf{B} :

$$\mathbf{B} = \nabla \times \left(\frac{\Phi}{2\pi r \sin \theta} \hat{\mathbf{e}}_\varphi \right). \quad (52)$$

The components of the poloidal magnetic field, in nondimensional units, are given by

$$b_x = \frac{1}{x^2 \sin \theta} \frac{\partial \phi}{\partial \theta}, \quad \text{and} \quad b_\theta = -\frac{1}{x \sin \theta} \frac{\partial \phi}{\partial x}. \quad (53)$$

Comparing these definitions with equations (21), and using the definition of β , eq. (24), one sees that there is a simple relation between the flux and the stream function given by

$$d\phi = \beta d\psi \quad (54)$$

Thus, the parametric equation for ψ , eq. (49), simply states that

$$\phi = \phi_*(1 - \cos \theta), \quad (55)$$

where $\phi_* = \phi(\pi/2)$ (just above the midplane) is the nondimensional magnetic flux trapped in the central source. In fact, ϕ_* labels the flux of the separatrix (see Figure 1). Moreover, the normalization eq. (50) and eq. (54) give

$$\bar{\beta} = -\frac{\phi_*}{m_0(1 + H_0)}. \quad (56)$$

Since every field line that lies interior to the separatrix threads the mass point at the center, one has the immediate identification that

$$\lambda_* = -\bar{\beta}^{-1} = \frac{m_0(1 + H_0)}{\phi_*}, \quad (57)$$

where λ_* is the nondimensional mass-to-flux ratio of the central star defined as

$$\lambda_* \equiv \frac{2\pi G^{1/2} M_*}{\Phi(r, \pi/2)}. \quad (58)$$

To summarize, the solution for small x consists of streamlines which are radial but non-uniformly distributed in θ . The θ dependence of both ψ and α is determined by the mass loading of field lines represented by $\beta(\psi)$, assumed to be known from the matching to the outer collapse solution. According to eqs. (21) and (45), the radial velocity is just free-fall, i.e.,

$$v_x = -\left[\frac{2m_0(1 + H_0)}{x}\right]^{1/2}. \quad (59)$$

By eq. (24), the magnetic field is that of a split monopole at the origin,

$$b_x = \frac{\phi_*}{x^2}, \quad (60)$$

as inferred by A03a,b. In physical units, the magnetic field of the split monopole is

$$B_r = \phi_* \frac{a^3 t}{G^{1/2} r^2}, \quad (61)$$

and is maintained by a current sheet in the equatorial plane, with current density in the azimuthal direction

$$J_\varphi = \frac{cB_r}{2\pi r} \delta(\theta - \pi/2). \quad (62)$$

Since the radial velocity increases as $v_x \propto x^{-1/2}$, while the (nondimensional) Alfvèn speed increases much faster, $v_A = b_x/\alpha^{1/2} \propto x^{-5/4}$, the flow asymptotically becomes highly subalfvènic, consistent with our assumption for A in eq. (43).

6. Case with rotation ($j \neq 0$).

In the case $j = 0$, the balance across and along streamlines is achieved by terms of order x^{-2} (see eq. 43 and 44). Multiplying eq. (34) by A , and eq. (39) by A^2 , one can show that the highest-order balance of the G-S and Bernoulli equations for $j \neq 0$ is unchanged. Thus, the non-rotating solution for the density α and the radial velocity and magnetic field, v_x and b_x , derived in the previous Section remains valid for $x \ll 1$, for any value of j . This is consistent with the findings of A03b that the isodensity contours and poloidal field (stream) lines are the same to zeroth approximation in the rotating and non-rotating case for small x .

Using eq. (37) together with the equation of continuity, eq. (17), the conservation of total angular momentum, $\nabla \cdot (\alpha \mathbf{v} j) = 0$, can be written as

$$\nabla \cdot (\alpha \mathbf{v}_p j_g) = \nabla \cdot (\mathbf{b}_p b_\varphi x \sin \theta) \quad (63)$$

where the gas specific angular momentum is $j_g = x \sin \theta v_\varphi$. This equation can be integrated over the upper hemisphere as

$$\int \alpha j_g \mathbf{v}_p \cdot d\mathbf{S} = \int x \sin \theta b_\varphi \mathbf{b}_p \cdot d\mathbf{S}, \quad (64)$$

where $d\mathbf{S} = 2\pi x^2 \sin \theta d\theta \hat{\mathbf{e}}_x$. The left hand side is rate of change of the gas specific angular momentum and the right hand side is the magnetic torque. Given our inner solution, the integral on the left hand side is $\propto xv_\varphi$ and the magnetic torque is $\propto x^{-1/2}v_\varphi$. Thus, the magnetic torque eventually dominates, decreasing the net gas angular momentum and forcing the azimuthal velocity to deviate from the $v_\varphi \propto x^{-1}$, behavior valid in the absence of magnetic torques. As discussed above, for small x the flow becomes subalfvènic ($\alpha\beta^2 \gg 1$). Thus, eq. (38) for the azimuthal velocity, together with eq. (40), implies that along each streamline $v_\varphi \propto x^{1/2}$, i.e., the azimuthal velocity decreases to zero at the origin. The long lever arm associated with the divergently strong split monopole field yields highly

efficient magnetic-braking, causing the gas to spiral into the central star without forming a centrifugally supported disk, as suggested by A03b.

Finally, from eq. (24), one can obtain the toroidal magnetic field component $b_\varphi \propto x^{-1}$, that increases with decreasing radius more slowly than the poloidal component b_x (eq. (60)). Thus, the winding of the field ($b_\varphi/b_x \propto x$) goes to zero as $x \rightarrow 0$, where the field geometry is dominated by the split monopole at the origin. Thus, in our treatment, reconnection of the poloidal magnetic field because of the sheet current that prevails in the magnetic midplane is more important than reconnection of the toroidal component that results because of the spinup of inflowing matter. In realistic circumstances, this state of affairs may change after the poloidal field is nearly entirely dissipated and a centrifugal disk is formed that can wind up relatively weak fields into a predominantly toroidal configuration.

Figure 2 summarizes the results of this Section and illustrates qualitatively the behavior of the azimuthal velocity in the equatorial plane of a collapsing magnetized cloud. We stress that different choices of the mass-loading of field lines specified by the function $\beta(\psi)$ would merely change the details of when and where the maximum rotational velocity is reached in the inflow solution, not the fact that the inflowing matter eventually loses all its specific angular momentum. In the next section, adopting a specific collapse model, we will show quantitatively that the region where magnetic braking by the split monopole becomes dominant over angular momentum conservation is generally larger than the size of a centrifugally supported disk formed in the absence of magnetic torques.

7. Matching to the outer collapse solution

We can match our inner collapse solution $x \ll 1$ to the outer collapse solution via the mass-loading function, $\beta(\psi)$, and the specific total angular momentum, $j(\psi)$. We use the simulations of A03a to perform this asymptotic matching. The exercise is nontrivial since collapse simulations with very high grid resolution are required to provide the “inner limit of the outer solution,” onto which we wish to match the “outer limit of the inner solution.” For our purposes, there is a further problem with the boundary condition imposed by Allen and co-workers on the radial field, namely $b_x = 0$ at $\theta = \pi/2$. This boundary condition, appropriate to the outside of the separatrix, is in conflict with the magnetic field configuration inside of the separatrix (that becomes the split monopole solution at small x) depicted in Figure 1. In fact, unlike the analytic work, it is numerically impossible to allow a current sheet at the equator (where b_x is discontinuous at the midplane) since this configuration is unstable to magnetic reconnection via numerical diffusion (see, e.g., Figure 4 of Galli & Shu 1993b). In spite of these drawbacks, we use the numerical β obtained from the simulations of

A03a to apply to our models, trusting the conservation principle associated with field freezing to yield the correct mass-to-flux loading for all colatitudes except close to the equator.

In Figure 3 the logarithm of $|\beta|$ is plotted as a function of the normalized flux, $\xi = \phi/\phi_*$, for different values of H_0 increasing from bottom to top. The points are the results of the simulations. The broken lines are fits given by

$$-\beta_{H_0} = b \exp(-c\xi) \xi^{-H_0} (1 - \xi^4)^2 + H_0, \quad (65)$$

where $b = H_0^{0.2} \exp(3.3H_0)$ and $c = 1.6 + 2.3H_0$. These broken lines yield a good representation of the numerical data for all angles except those close to the equator, $\xi = 1$. The numerical β goes to zero due to the boundary condition discussed above (see eq. 24). The analytic solution requires β to be finite and $\beta' = 0$ at the midplane; otherwise the density gradient will become discontinuous.

Note that the function β diverges at the pole ($\theta = 0$) because in the starting toroids the density there goes to zero. Finally, since the numerical simulations give $\beta(\phi)$, not $\beta(\psi)$, we use the fact that $d\psi = \phi_* d\xi / \beta(\xi)$, to obtain from eq. 54) and (57)

$$\lambda_* = - \int_0^1 \frac{d\xi}{\beta(\xi)}. \quad (66)$$

The numerical values of λ_* can be determined only approximately, owing to the effects of the boundary condition at the midplane on the numerical values of β . Roughly, we obtain $\lambda_* \approx 3\text{--}4$ for $H_0 = 0.125$, $\lambda_* \approx 2.4\text{--}2.7$ for $H_0 = 0.25$, $\lambda_* \approx 1.2\text{--}1.7$ for $H_0 = 0.5$, and $\lambda_* = 1.0\text{--}1.3$ for $H_0 = 1$. These values are closer to the mass-to-flux ratio λ_r than they are to λ as tabulated in Table 1 of Li & Shu (1996). The former applies for the initial state of an isopedic toroid when one integrates for the mass along flux tubes for given H_0 only to a spherical surface of radius r , whereas the latter applies if one integrates all the way out to ∞ . For given trapped flux, we can expect mass accumulation to behave in the latter case only in the case of complete flattening, $H_0 \rightarrow \infty$. For more modest values of H_0 , we can expect a more nearly spherical reach for both mass and flux when the configuration collapses, yielding the closer correspondence of λ_* to λ_r .

In contrast, T Tauri stars have observed values of $\lambda_* \approx 10^3\text{--}10^4$ (see e.g. Johns-Krull et al. 2004), implying that the assumption of field-freezing must break down at some point in the star formation process (Shu et al. 2006). As expected, according to our ideal MHD solution the magnetic field trapped in the central protostar exceeds observed stellar fields by three-four orders of magnitude. The four panels of Figure 4 show our inner collapse solutions in self-similar coordinates for the four values of H_0 given above. The heavy solid contours in each panel are isodensity contours and the radial lines are the magnetic field lines (which

coincide with the streamlines). The arrows show the velocity field at different radii. The dynamic pseudodisks that result may bear comparison with observations of young protostars before they have developed full disks (Hogerheijde 2004).

Quantitatively, the condition for subalfvènic radial flow $\alpha\beta^2 > 1$, necessary for strong magnetic braking according to the results described in the previous section, is valid in a region $x < x_A(\theta)$ where x_A is the nondimensional Alfvèn radius. With our asymptotic expressions for v_x and b_x (eq. 59 and 60) and our fitting formula for β (eq. 65), it is possible to estimate the value of x_A on the midplane ($\theta = \pi/2$), obtaining $x_A \approx 0.085, 0.18$, and 0.45 for $H_0 = 0.125, 0.25$ and 0.5 . These values can be compared with the expected disk radius for the collapse of a non-magnetized Toomre–Hayashi toroid, $x_d \approx 0.25v_0^2$, where v_0 is the (uniform) rotation velocity in units of the isothermal sound speed a (A03b). The magnitude of v_0 for molecular cloud cores ranges from 0.03 to 0.4, with typical value $v_0 \approx 0.1$ (Goodman et al. 1993), in which case $x_d \approx 0.0025$. Thus, $x_d \ll x_A$ even for weakly magnetized clouds ($H_0 = 0.125\text{--}0.5$), and the formation of a centrifugally supported disk cannot take place. Even for the weakly-magnetized, fast-rotating cloud model with $v_0 = 0.5$ and $H_0 = 0.25$ considered by A03b (see their Fig. 7), the radius of the disk that would be formed in the absence of magnetic torques, $x_d \approx 0.063$, is about 3 times smaller than the Alfvèn radius, $x_A \approx 0.18$, explaining why A03b did not observe the formation a centrifugal disk even in this extreme model.

8. Comparison with previous work

The process of magnetic braking has been usually considered in the context of the quasi-static evolution of a molecular cloud core (e.g. Gillis, Mestel & Paris 1974, 1979; Mouschovias & Paleologou 1979). Recent semi-analytical calculations and numerical simulations have extended these works to follow the increase of density towards the formation of an optically thick core (Tomisaka 2002, Machida et al. 2005a,b) and through the formation of a point-mass into the protostellar accretion phase (Li & Shu 1997; Ciolek & Königl 1998; Contopoulos, Ciolek & Königl 1998; A03a,b). Krasnopolksy & Königl (2002) extended the semi-analytical calculations by Contopoulos et al. (1998) to study the collapse of magnetized, rotating, thin disks surrounded by an external medium with specified physical properties. They found that the decoupling of matter and magnetic field (by ambipolar diffusion) is carried by an outward propagating shock, as first suggested by Li & McKee (1996), and the infalling rotating material is halted by a centrifugal shock inside which a centrifugal disk is established. The formation and radial extent of the centrifugal disk depend on two main parameters: the ratio δ of the azimuthal and vertical components of the magnetic field at the disk surface and the

Alfven speed in the external medium, both controlling the importance of magnetic braking during the collapse. In the ideal MHD case (no ambipolar diffusion), for models with a large winding of the magnetic field ($\delta = 10$) they obtain complete braking, i.e. no centrifugal disk is formed. As in our case, the horizontal flow approaches free-fall onto the central mass and the magnetic field of the protostar is that of a split monopole at the origin. However, our model differs from theirs in that our collapsing cores are 3-D with axial symmetry and we do not include an external medium. The magnetic braking is due to the field lines that connect the inner region, $x \ll 1$, with the rest of the collapsing cloud and thus the magnetic field winding and magnetic braking are calculated self-consistently (through the functions j and β). In addition, we find that the radial component of the field largely dominates over the azimuthal component at small radii, so the winding of the field is never as severe as assumed by Krasnopol'sky & Königl (2002).

9. Summary and conclusions

We have examined the properties of the inner regions of an ideally magnetized, isothermal, rotating cloud undergoing gravitational collapse. The density distribution and the poloidal velocity field in the collapse solution approach free-fall forms, while the trapped magnetic field rooted in the central protostar acquires a split monopole configuration. An analytic solution can be obtained for the central regions if numerical simulations are used to obtain the loading function that determines how much mass is coming down a given field line. For illustrative purposes, we have adopted the mass loading function β from the numerical simulations of A03a. We note, however, that the properties of our collapse solution discussed in Sect. 5 and Sect. 6 are general, and do not depend on these particular numerical simulations.

The long lever arm associated with the strong field is able to brake the rotation of the infalling gas so efficiently that the azimuthal velocity goes to zero at the origin. In other words, the infalling gas spirals directly into the center without the formation of a centrifugally supported disk. Although this conclusion rigorously holds only for the particular class of collapse models considered in this paper, the assumption of self-similarity helps to bring out the dependence of our results on the fundamental physical parameters of the problem, like the cloud's mass-to-flux ratio and rotation rate, suggesting a broader validity of our main conclusions. Thus, the catastrophic magnetic braking discussed in Sect. 6, for example, does not depend on the particular choice of the outer collapse solution but follows directly from the ideal MHD equations. This work therefore proves that magnetic field dissipation is a crucial ingredient to allow the formation of the circumstellar disks observed around young

stars. It also yields departure points for calculations which include outflow in the presence of inflow (Lizano et al. 2006, in preparation) or modifications introduced by the effects of finite resistivity (Shu et al. 2006).

DG and SL acknowledge financial support from the Theoretical Institute for Advanced Research in Astrophysics (TIARA), CRyA/UNAM, DGAPA/UNAM and CONACyT (Mexico), and INAF-Osservatorio Astrofisico di Arcetri (Italy), where part of the research presented in this paper was done. The authors are also grateful to members and staff of these institutions for warm hospitality. The research work of FS and AA in Taiwan is supported by the grant NSC92-2112-M-001-062.

REFERENCES

Allen, A., Shu, F. H., & Li, Z.-Y. 2003, *ApJ*, 599, 351

Allen, A., Li, Z.-Y., & Shu, F. H. 2003, *ApJ*, 599, 363

Ciolek, G. E., & Königl, A. 1998, *ApJ*, 504, 257

Contopoulos, I., Ciolek, G. E., & Königl, A. 1998, *ApJ*, 504, 247

Galli, D., & Shu, F. H. 1993a, *ApJ*, 417, 220

Galli, D., & Shu, F. H. 1993b, *ApJ*, 417, 243

Gillis, J., Mestel, L., & Paris, R. B. 1974, *Ap&SS*, 27, 167

Gillis, J., Mestel, L., & Paris, R. B. 1979, *MNRAS*, 187, 311

Goodman, A. A., Benson, P. J., Fuller, G. A., & Myers, P. C. 1993, *ApJ*, 406, 528

Hogerheijde, M. 2004, in *Star Formation at High Angular Resolution*, IAU Symp. 221, eds. M. Burton, R. Jayawardhana, & T. Bourke (Kluwer), p. 361

Johns-Krull, C. M., Valenti, J. A., & Saar, S. H. 2004, *ApJ*, 617, 1204

Krasnopolsky, R., Königl, A. 2002, *ApJ*, 580, 987

Li, Z., & Shu, F. H. 1996, *ApJ*, 472, 211

Li, Z., & Shu, F. H. 1997, *ApJ*, 475, 237

Machida, M. N., Matsumoto, T., Tomisaka, K., & Hanawa, T. 2005, MNRAS, 362, 369

Machida, M. N., Matsumoto, T., Hanawa, T., & Tomisaka, K. 2005, MNRAS, 362, 382

Mestel, L., & Spitzer, L. 1956, MNRAS, 116, 503

Mouschovias, T. C., & Paleologou, E. V. 1979, ApJ, 230, 204

Shafronov, V. D. 1966, Rev. Plasma Phys., 2, 103

Shu, F. H., Najita, J., Ruden, S. P., & Lizano, S. 1994, 429, 797

Shu, F. H., Galli, D., Lizano, S., Cai, M. 2006, ApJ, submitted

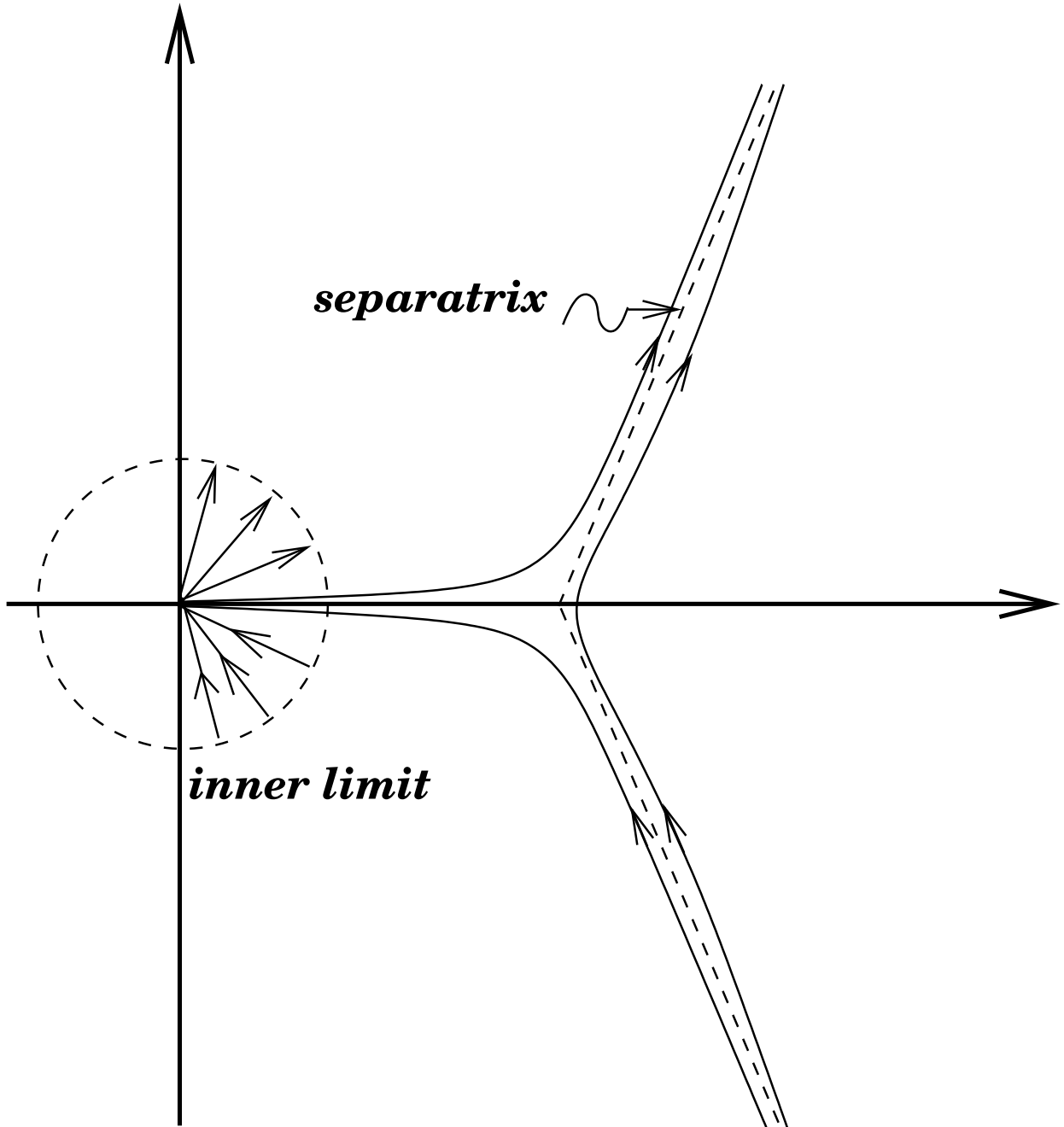


Fig. 1.— Geometry of the magnetic field in a collapsing magnetized cloud. The separatrix (dashed curve) separates field lines which have been pulled into an accreting protostar (at the origin of the coordinate system) from field lines tied to matter in the infalling envelope. A dashed circle indicates the inner region with nondimensional radius $x \ll 1$ studied in this paper, where magnetic field lines are asymptotically radial.

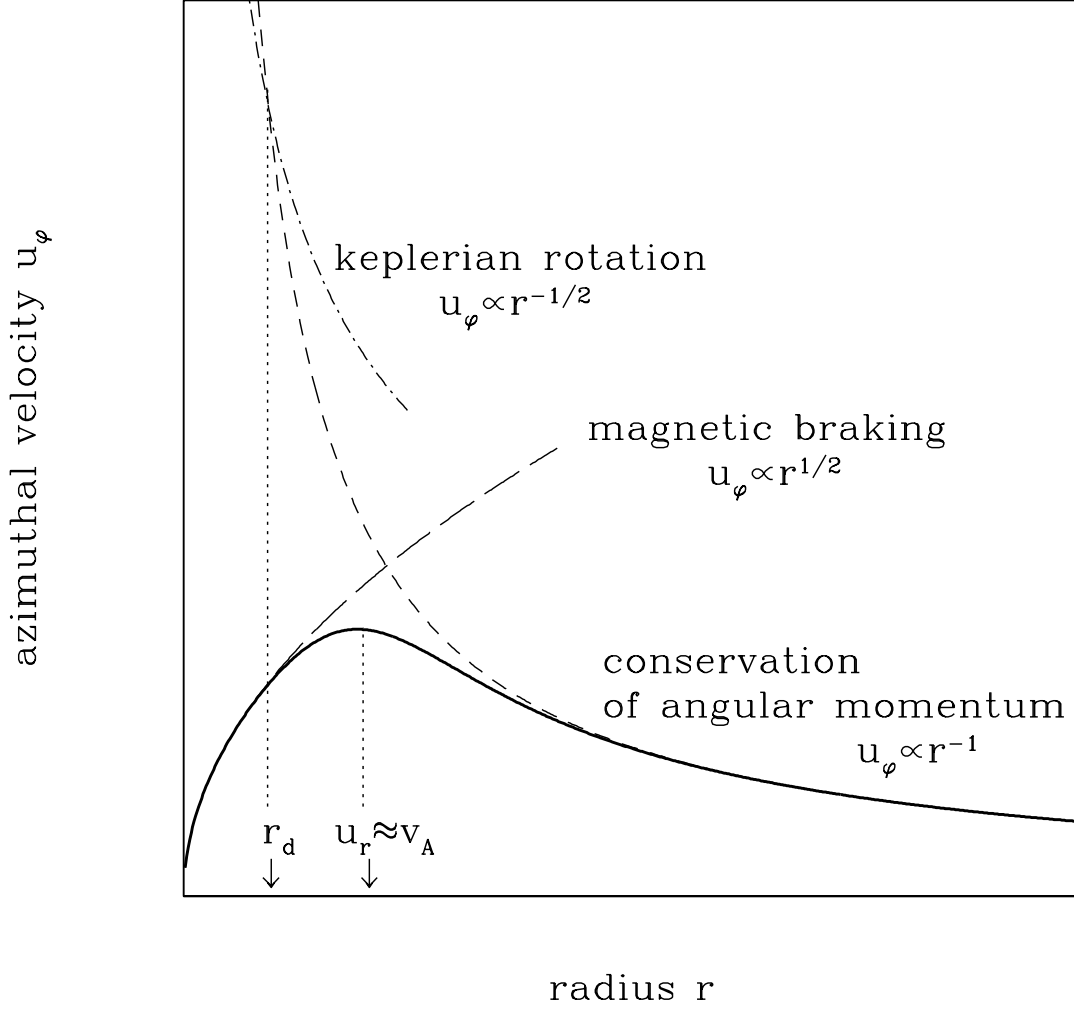


Fig. 2.— Schematic behavior of the azimuthal velocity u_ϕ (*solid curve*) in the equatorial plane of a collapsing cloud as function of the distance r from the central protostar. In the absence of magnetic torques, a centrifugally supported disk is formed inside a radius r_d , where the azimuthal velocity increasing as r^{-1} becomes equal to the keplerian velocity around the protostar ($\propto r^{-1/2}$). In contrast, the magnetic torque associated with the split monopole field of the central protostar reduces the angular momentum of the infalling gas, constraining the azimuthal velocity to decrease as $r^{1/2}$ at small radii. Magnetic braking becomes dominant over angular momentum conservation when the infall velocity u_r becomes smaller than the local Alfvèn speed v_A .

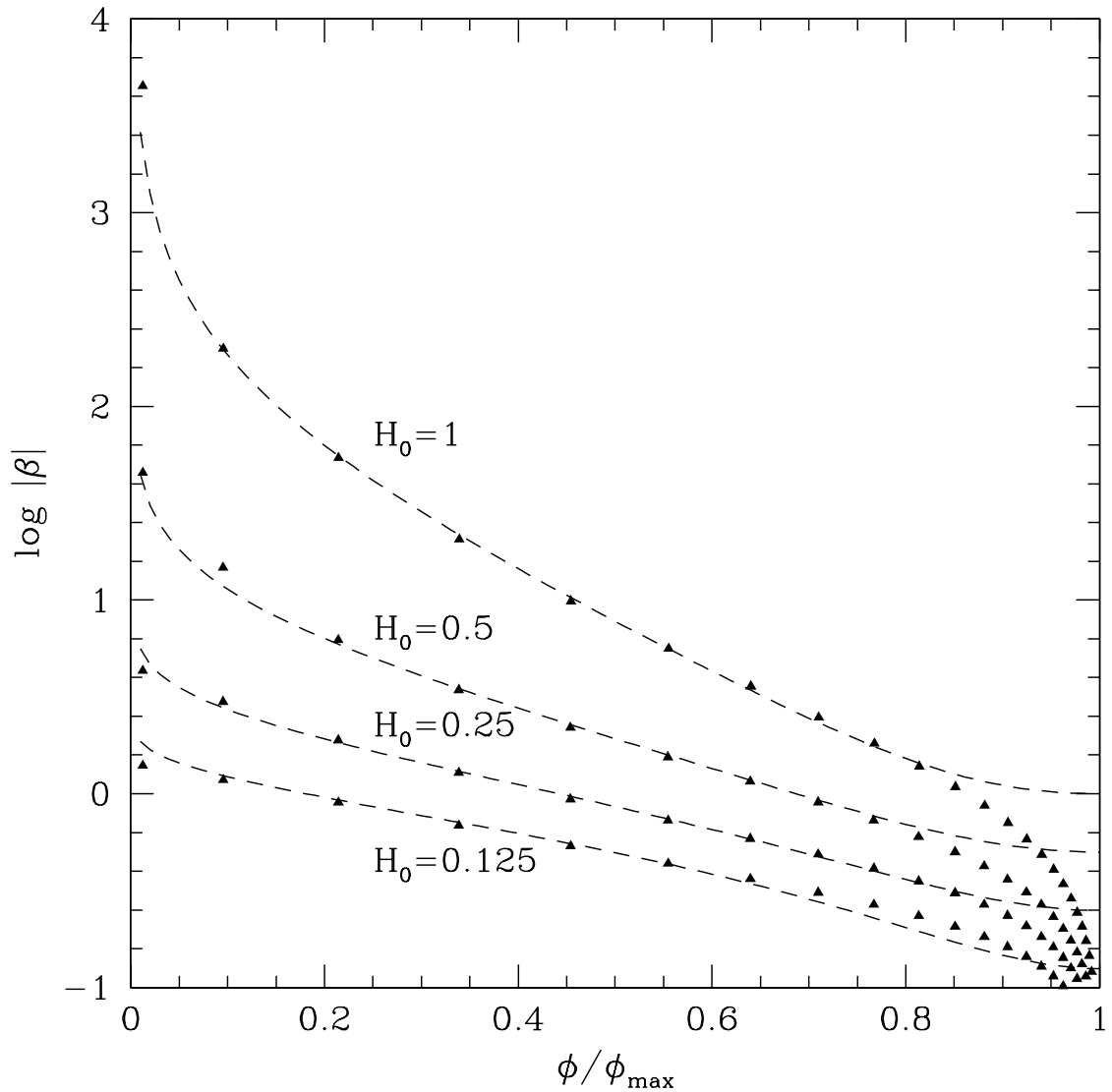


Fig. 3.— The function β related to the mass loading of field lines (eq. 24), plotted as function of the normalized flux $\phi / \phi_{\star} = 1 - \cos \theta$. The *triangles* show the function β computed numerically by A03a for $H_0 = 0.125, 0.25, 0.5$ and 1 ; the *dashed curves* are analytical fits given by eq. (65).

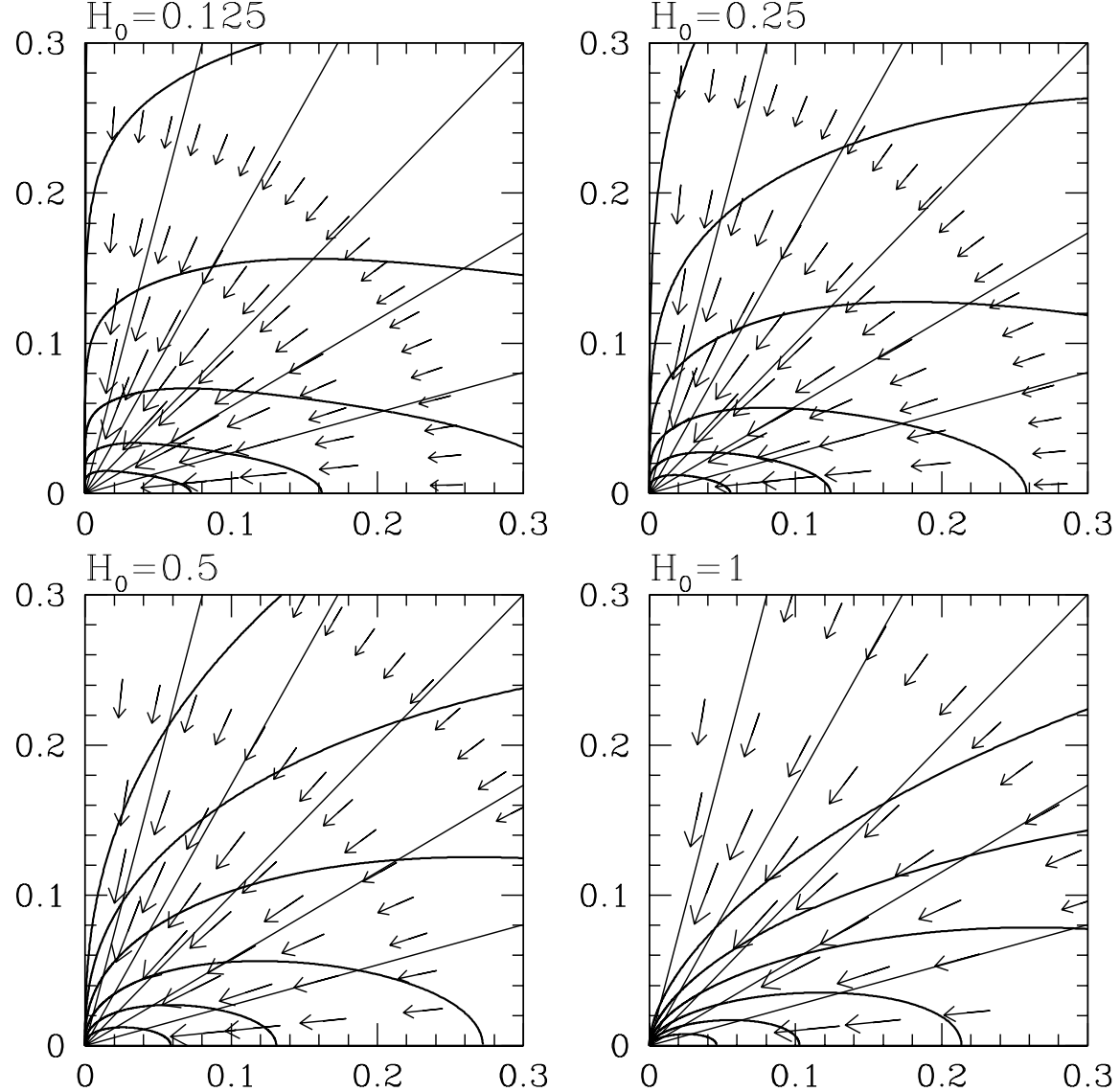


Fig. 4.— Inner collapse solutions (valid asymptotically for $x \ll 1$) obtained for the values of the parameter H_0 and the functions β shown in Figure 3. The horizontal and vertical axis in each panel are the cylindrical self-similar coordinates, $\varpi = x \sin \theta$ and $z = x \cos \theta$. The *heavy solid contours* in each panel are isodensity contours for the levels $\alpha = 100, 30, 10, 3, 1$ and 0.3. The *thin solid lines* are the magnetic field lines (which coincide with the streamlines). The *arrows* show the velocity field at different radii, logarithmically spaced in the velocity interval [2.5, 6].